HIGH-RESOLUTION SPECTRAL IMAGE RECONSTRUCTION BASED ON COMPRESSED DATA FUSION

Óscar Espitia[(1)], *Henry Arguello*[(1)], *Jean-Yves Tourneret*[(2)]

[(1)]Universidad Industrial de Santander, Colombia, [(2)]University of Toulouse, IRIT/INP-ENSEEIHT

ABSTRACT

Compressive spectral imagers drastically reduce the number of sampled pixels by performing linear combinations of coded spectral information. However, compressing information with simultaneously high spatial and high spectral resolutions demands expensive high-resolution sensors. This work introduces a model allowing compressive data from high spatial/low spectral and low spatial/high spectral resolution sensors to be fused. The sensing matrix of this model is designed carefully to be incoherent with the dictionary associated with the unknown image. Based on this model, the compressive fusion process is formulated as an inverse problem that minimizes an objective function defined as the sum of a quadratic data fidelity term and smoothness and sparsity regularization penalties.

Index Terms— Spectral imaging, compressive sampling, data fusion, remote sensing

1. INTRODUCTION

Remote sensing imagers deliver images with either high spatial/low spectral or high spectral/low spatial resolutions. However, some applications involving feature detection and classification require images with both high spectral and high spatial resolutions [1]. On the other hand, most imaging systems deliver data with a significant redundancy, which can be reduced by using compressive sensing (CS) [2, 3]. CS is based on the fact that many natural signals can be represented with few coefficients in some basis and can thus be compressed efficiently. It has been shown that the use of appropriate sensing matrices allows the performance of signal reconstruction methods to be close to the one obtained without using CS [4]. However, obtaining low-cost compressed measurements with high spatial and high spectral resolutions is a challenging problem.

This paper introduces a model allowing images acquired with compressive sensing with different spatial and spectral resolutions to be reconstructed. We argue that the use of compressive measurements with appropriate sensing matrices can lead to high-quality image reconstruction and that compressive measurements have favorable properties to solve the multisensor fusion problem. The images considered in this work are assumed to result from spectral and/or spatial degradations of a high spectral and high spatial resolution hyperspectral (HS) image (to be recovered) and from a CS operation.

The HS image of interest is stacked into a column vector $\mathbf{f} = [f_1, ..., f_{N_H}]^T \in \mathbb{R}^{N_H}$, where $N_H = M \times N \times L$, $M \times N$ is the number of image pixels and L is the number of spectral bands. We assume that $\mathbf{f}$ can be decomposed as $\mathbf{f} = \mathbf{\Psi}\mathbf{x}$, where $\mathbf{x} \in \mathbb{R}^{N_H}$ contains only $S \ll N_H$ nonzero elements and $\mathbf{\Psi} \in \mathbb{R}^{N_H \times N_H}$ is an operator expressing the fact that the image is sparse in a given domain (e.g., in the wavelet domain). The noiseless observations are HS and multispectral (MS) compressed measurements denoted as $\mathbf{f}_H = \mathbf{\Phi}_1\mathbf{B}\mathbf{f} = \mathbf{\Phi}_H\mathbf{f}$ and $\mathbf{f}_M = \mathbf{\Phi}_2\mathbf{L}\mathbf{f} = \mathbf{\Phi}_M\mathbf{f}$, where $\mathbf{B} \in \mathbb{R}^{M_h N_h L \times N_H}$ ($M_h N_h \ll MN$) is an operator associated with spatial blurring and downsampling, $\mathbf{L} \in \mathbb{R}^{MNL_m \times N_H}$ ($L_m \ll L$) is a filtering operator transforming the spectral content of the reference image into the spectral bands of the MS image and $\mathbf{\Phi}_1 \in \mathbb{R}^{P \times M_h N_h L}$, $\mathbf{\Phi}_2 \in \mathbb{R}^{Q \times NML_m}$ are compressive matrices [3, 4, 5]. Note that $\mathbf{\Phi}_H \in \mathbb{R}^{P \times N_H}$ and $\mathbf{\Phi}_M \in \mathbb{R}^{Q \times N_H}$ are the respective HS and MS CS matrices that perform both compression and decimation operations, simultaneously.

The problem addressed in this paper consists of estimating the unknown image $\mathbf{f}$ from the observations $\mathbf{y}_H = \mathbf{f}_H + \mathbf{n}_H$ and $\mathbf{y}_M = \mathbf{f}_M + \mathbf{n}_M$, where $\mathbf{n}_H$ and $\mathbf{n}_M$ are the HS and MS noise vectors. Assuming that $\mathbf{f}$ is sparse in the $\mathbf{\Psi}$ domain, it is known that an appropriate choice of the numbers of projections $P, Q \ll N_H$ and of the sensing matrices $\mathbf{\Phi}_H$ and $\mathbf{\Phi}_M$ allows an accurate recovery of the image $\mathbf{f}$ from $\mathbf{y}_H$ and $\mathbf{y}_M$ [3, 4, 5]. Note that the observation model defined by $\mathbf{y}_H$ and $\mathbf{y}_M$ is similar to the one introduced in [6], except that the unknown image $\mathbf{f}$ has been vectorized. However, we exploit here the sparsity of the matrices $\mathbf{\Phi}_1$ and $\mathbf{\Phi}_2$ for fusing spectral images with a reduced computational cost. Note that sparsity guarantees that the inverse problem consisting of estimating $\mathbf{f}$ from $\mathbf{y}_H$ and $\mathbf{y}_M$ is well-posed [7].

The fusion of images with different spatial and spectral resolutions is formulated as an inverse problem that minimizes an appropriate objective function. This objective function is built as the sum of a quadratic data fidelity term and smoothness and sparsity regularizations. To ensure a good performance of the proposed image reconstruction method, the coded aperture snapshot spectral imager (CASSI) [5, 8] is used to obtain the compressive projections and a sensing matrix design approach is introduced.

The outline of this paper is as follows: Section 2 summarizes some basic elements about the CASSI model and the design of the suggested sensing matrix. Section 3 formulates the fusion of HS and MS images as the inverse problem investigated in this work. Experimental results are presented in Section 4, showing that the reconstructed images are very close to the high-resolution reference images. Concluding remarks are finally reported in Section 5.

2. THE CASSI SYSTEM

In this work, we focus on the CASSI system, which has shown interesting properties for image reconstruction [8]. The CASSI system encodes the 2D spatial information of a scene by using a block-unblock patterned mask. The coded spatial projections are then spectrally shifted by using a dispersive element. A 2D sensor finally detects these coded and shifted projections. The image intensity of the detector in the the kth snapshot is given by

$$Y^k_{i,j} = \sum_{l=0}^{L-1} F_{i,(j-l),l} T^k_{i,(j-l)} + n^k_{i,j} \quad (1)$$

where $\mathbf{F} = \{F_{i,j,l}\}$ is the discretized spectral image, $\mathbf{T} = \{T^k_{i,j}\}$ is the discretized patterned mask used for the kth snapshot (with $T^k_{i,j} \in \{0,1\}$), and n is the noise of the sensing system [5]. Equation (1) can be rewritten using matrix/vector notations as $\mathbf{y}^k = \mathbf{\Phi}^k \mathbf{f} + \mathbf{n}^k$, where $\mathbf{y}^k \in \mathbb{R}^{M(N+L-1)}$ and $\mathbf{f}$ is a vector obtained by vectorization of $\mathbf{F}$, leading to the classical linear system $\mathbf{y} = \mathbf{\Phi f} + \mathbf{n}$, where $\mathbf{\Phi}$ corresponds to the global system. Fig. 1 illustrates how the structured matrix $\mathbf{\Phi}$ is constructed for the CASSI system.

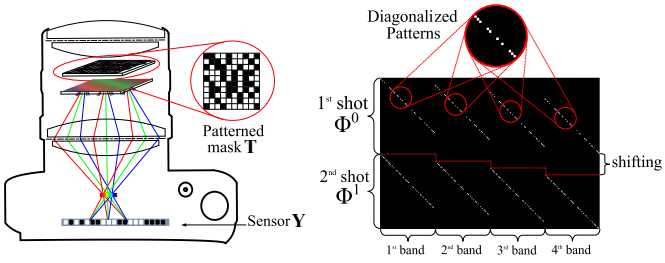

Fig. 1. CASSI measurement matrix. $\mathbf{\Phi}$ consists of a set of vectorized patterned masks in diagonal form, that repeat along the horizontal direction, such that one spatial dimension is shifted downward, as many times as the number of spectral bands.

2.1. HS and MS CASSI measurements

This paper uses CASSI measurements to build the HS and MS data. Fig. 2 (Top) shows the structure of the CASSI sensing matrix $\mathbf{\Phi}_H$. Note that each row of this matrix performs a linear combinations of p^2 adjacent pixels, which means that the scene projected onto this matrix, besides being compressed, is degraded spatially by a factor p (e.g., $p = 2$ in Fig. 2 (Top)). The entries of the matrix $\mathbf{\Phi}_H$ are defined as

$$\Phi_{H_{i,j}} = \begin{cases} t_H\left(a_j + \frac{M}{p} b_j + \frac{M^2}{p^2} c_j\right) & \text{if } i = a_j + \frac{M}{p}(b_j + c_j) \\ 0 & \text{otherwise} \end{cases} \quad (2)$$

where $\boldsymbol{t}_H = [t_H(1), ..., t_H(\frac{MN}{p^2})]^T$ is a vectorized patterned mask $\mathbf{T}$ for $\mathbf{\Phi}_H$, $a_j = \lfloor \frac{j}{p} \rfloor$, $b_j = \lfloor \frac{j}{pM} \rfloor - \lfloor \frac{j}{M} \rfloor$, $c_j = \lfloor \frac{j}{M^2} \rfloor$, and $\lfloor . \rfloor$ denotes the integer part. Similarly, Fig. 2 (Bottom) shows the structure of the CASSI sensing matrix $\mathbf{\Phi}_M$ used for the MS measurements. Note that each row of this matrix performs a linear combination between the pixels of the q adjacent bands, which means that the spectral resolution of the MS sensor is q times smaller than the one of the reference scene (e.g., $q = 4$ in Fig. 2 (Bottom)). The entries of the matrix $\mathbf{\Phi}_M$ can be written as follows

$$\Phi_{M_{i,j}} = \begin{cases} t_M\left(i - r_j(MN - M)\right) & \text{if } i = j \bmod (NM) + M\lfloor \frac{j}{qMN} \rfloor \\ & \text{and } j - r_j M \geq 0 \\ 0 & \text{otherwise} \end{cases} \quad (3)$$

where $\boldsymbol{t}_M = [t_M(1), ..., t_M(NM)]^T$ is a vectorized patterned mask $\mathbf{T}$ for $\mathbf{\Phi}_M$, and $r_j = \lfloor \frac{j}{MN} \rfloor$.

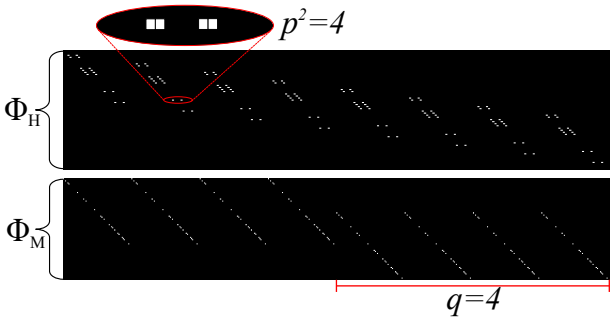

Fig. 2. HS and MS CASSI sensing matrices - $\mathbf{\Phi}_H$ and $\mathbf{\Phi}_M$

The sensing matrices $\mathbf{\Phi}_H$ and $\mathbf{\Phi}_M$ can be designed to achieve high-quality results for CS approaches [9, 10]. The design of the global system is clarified in the next subsection, exploiting the fact that both systems can sample the scene complementary.

2.2. Sensing matrix design

In CS theory, a suitable measurement matrix $\mathbf{\Phi}$ is desired to be as incoherent as possible with the sparse dictionary $\mathbf{\Psi}$ [4]. The mutual coherence of the Gram matrix $\mathbf{G} = (\mathbf{\Phi\Psi})^T(\mathbf{\Phi\Psi})$ is defined as the off-diagonal entry in $\mathbf{G}$ with the largest absolute magnitude. The sensing matrix can be optimized by minimizing the mutual coherence the $\mathbf{G}$. Consequently, considering that the dictionary is known, a sensing matrix can be chosen such that the corresponding Gram matrix is as close as possible to the identity [11], i.e.,

$$\mathbf{G} = \mathbf{\Psi}^T \mathbf{\Phi}^T \mathbf{\Phi\Psi} \approx \mathbf{I}. \quad (4)$$

Note that if the dictionary $\mathbf{\Psi}$ is an orthogonal basis ($\mathbf{\Psi}^T\mathbf{\Psi} = \mathbf{I}$), in order to have (4), it make sense to choose $\mathbf{\Phi}$ such that $\mathbf{\Phi}^T\mathbf{\Phi} \approx \mathbf{I}$. Thus, the design of the sensing matrix reduces to an appropriate choice of $\mathbf{\Phi}$. We propose to choose the matrix $\mathbf{\Phi}$ as a binary matrix containing only one 1 per column, in order to reduce the off-diagonal elements of $\mathbf{\Phi}^T\mathbf{\Phi}$. Denote as

$\boldsymbol{c} = [c_0, \cdots, c_{N_H-1}]^T$ the vector such that

$$c_j = \sum_{i=0}^{P-1} \Phi_{H_{i,j}} + \sum_{i=0}^{Q-1} \Phi_{M_{i,j}} \tag{5}$$

where c_j corresponds to the number of ones in the jth column of $\mathbf{\Phi}$, for $j = 0, ..., N_H - 1$, $N_H = MNL$ is the number of columns of the matrix Φ, $\Phi_{H_{i,j}}$ and $\Phi_{M_{i,j}}$ are the elements of the ith row and jth column of the sensing matrices $\mathbf{\Phi}_H$ and $\mathbf{\Phi}_M$, respectively. When each column of Φ contains exactly one 1 and all other values are 0, the matrix Φ satisfies the following relations

$$\sigma_c^2 = \frac{1}{N_H} \sum_{j=0}^{N_H-1} (c_j - \bar{c})^2 = 0, \quad \bar{c} = 1. \tag{6}$$

Since these conditions are too restrictive in practice, we propose to design the matrix $\mathbf{\Phi}$ by minimizing the variance σ_c^2 with the constraint $\bar{c} = 1$. Since the entries of $\boldsymbol{c}$ are binary, this problem can be solved using the direct binary search algorithm (see [12] for more details).

3. SOLVING THE CS-FUSION PROBLEM

In order to recover the high resolution datacube from the compressive measurements $\mathbf{y}_H$ and $\mathbf{y}_M$, we propose to solve the following optimization problem

$$\widehat{\mathbf{x}} = \arg \min_{\mathbf{x}} \frac{1}{2}||\mathbf{y_H} - \mathbf{\Phi}_H\mathbf{\Psi}\mathbf{x}||_2^2 + \frac{1}{2}||\mathbf{y_M} - \mathbf{\Phi_M}\mathbf{\Psi}\mathbf{x}||_2^2 + \phi_1(\mathbf{x}) \tag{7}$$

where the two first terms are the data fidelity terms associated with the HS and MS images and the last term is a penalty ensuring an appropriate regularization. The unknown image is then estimated as $\widehat{\mathbf{f}} = \mathbf{\Psi}\widehat{\mathbf{x}}$. After expanding the two quadratic terms in (7) and introducing $\mathbf{y} = [(\mathbf{y}_M)^T, (\mathbf{y}_H)^T]^T$, and the global system as $\mathbf{\Phi} = [(\mathbf{\Phi}_H)^T, (\mathbf{\Phi}_M)^T]^T$, problem (7) can be rewritten as

$$\widehat{\mathbf{f}} = \arg \min_{\mathbf{f}} \frac{1}{2}||\mathbf{\Phi}\mathbf{f} - \mathbf{y}||_2^2 + \phi_2(\mathbf{f}) \tag{8}$$

where $\phi_2(\mathbf{f}) = \phi_1(\mathbf{\Psi}^T\mathbf{f})$ is a penalty associated with the unknown image $\mathbf{f}$. The regularization term considered in this work is

$$\phi_2(\mathbf{f}) = \mu||\mathbf{f}||_{\text{TV}} + \tau||\mathbf{\Psi}^T\mathbf{f}||_1 \tag{9}$$

where $||\cdot||_{\text{TV}}$ and $||\cdot||_1$ are the TV and l_1 norms, respectively. This regularization attempts to preserve the smoothness of $\mathbf{f}$ in the spatial domain and the sparsity of the coefficients $\mathbf{x} = \mathbf{\Psi}^T\mathbf{f}$ in the domain of the representation basis $\mathbf{\Psi}$. An alternative way to solve (8) with the regularizer (9) is

$$\begin{aligned} \widehat{\mathbf{f}} = \arg\min_{\mathbf{f}} \quad & \frac{1}{2}||\mathbf{\Phi}\mathbf{f} - \mathbf{y}||_2^2 + \mu||\boldsymbol{\nu}^{(1)}||_{TV} + \tau||\boldsymbol{\nu}^{(2)}||_1 \\ \text{subject to} \quad & \boldsymbol{\mathcal{L}}\mathbf{f} - \boldsymbol{\nu}^{(1)} = 0 \\ & \mathbf{\Psi}\mathbf{f} - \boldsymbol{\nu}^{(2)} = 0 \end{aligned} \tag{10}$$

where $\nu^{(1)}$ and $\nu^{(2)}$ are auxiliary variables, resulting from the application of the alternating direction method of multipliers [13], and $\boldsymbol{\mathcal{L}}$ is an operator enforcing piecewise constant solutions associated with the TV regularizer (see [14] for more details). An approach for solving (10) is to minimize the augmented Lagrangian defined by

$$\begin{aligned} L(\mathbf{f}, \boldsymbol{\nu}^{(1)}, \boldsymbol{\nu}^{(2)}) = & \frac{1}{2}\|\mathbf{\Phi}\mathbf{f} - \mathbf{y}\|_2^2 + \mu\left\|\boldsymbol{\nu}^{(1)}\right\|_{TV} + \tau\left\|\boldsymbol{\nu}^{(2)}\right\|_1 \\ & + \frac{\rho}{2}\left\|\boldsymbol{\mathcal{L}}\mathbf{f} - \boldsymbol{\nu}^{(1)} + \mathbf{d}^{(1)}\right\|_2^2 + \frac{\rho}{2}\left\|\mathbf{\Psi}\mathbf{f} - \boldsymbol{\nu}^{(2)} + \mathbf{d}^{(2)}\right\|_2^2. \end{aligned} \tag{11}$$

For solving the fusion problem, we propose to minimize the function $L(\mathbf{f}, \boldsymbol{\nu}^{(1)}, \boldsymbol{\nu}^{(2)})$ alternatively with respect to (w.r.t.) $\mathbf{f}$, $\boldsymbol{\nu}^{(1)}$, and $\boldsymbol{\nu}^{(2)}$. This leads to Algorithm 1, where $\mathbf{f}_{\ell+1}$ is the updated term for $\mathbf{f}$ in line 4, obtained by differentiating

$$\begin{aligned} L(\mathbf{f}) = \quad & \frac{1}{2}\|\mathbf{\Phi}\mathbf{f} - \mathbf{y}\|_2^2 + \frac{\rho}{2}\left\|\boldsymbol{\mathcal{L}}\mathbf{f} - \boldsymbol{\nu}^{(1)} + \mathbf{d}^{(1)}\right\|_2^2 + \\ & \frac{\rho}{2}\left\|\mathbf{\Psi}\mathbf{f} - \boldsymbol{\nu}^{(2)} + \mathbf{d}^{(2)}\right\|_2^2 \end{aligned} \tag{12}$$

w.r.t. $\mathbf{f}$ and forcing it to be zero. As (11) is not differentiable w.r.t. $\boldsymbol{\nu}^{(1)}$ and $\boldsymbol{\nu}^{(2)}$, we update these parameters using the soft thresholding operations described in lines 5 and 6 of Algorithm 1, which result from the computation of appropriate proximal operators (see [13, 14] for details).

Algorithm 1 Compressive fusion procedure

1: **Initialization**: set $\mathbf{\Phi}$, $\mathbf{\Psi}$, ($\mathbf{f}_0$, $\boldsymbol{\nu}_0^{(1)}$, $\boldsymbol{\nu}_0^{(2)}$, $\mathbf{d}_0^{(1)}$,$\mathbf{d}_0^{(2)}$) to zero, μ, τ, ρ.
2: **repeat**
3: $\quad \mathbf{r}_\ell = \mathbf{\Phi}^T\mathbf{y} + \rho\left(\boldsymbol{\mathcal{L}}^T\left(\boldsymbol{\nu}_\ell^{(1)} - \mathbf{d}_\ell^{(1)}\right) + \mathbf{\Psi}^T\left(\boldsymbol{\nu}_\ell^{(2)} - \mathbf{d}_\ell^{(2)}\right)\right)$
4: $\quad \mathbf{f}_{\ell+1} = \left(\mathbf{\Phi}^T\mathbf{\Phi} + \rho\left(\boldsymbol{\mathcal{L}}^T\boldsymbol{\mathcal{L}} + \mathbf{\Psi}^T\mathbf{\Psi}\right)\right)^{-1}\mathbf{r}_\ell$
5: $\quad \boldsymbol{\nu}_{\ell+1}^{(1)} = \text{Soft}\left(\boldsymbol{\mathcal{L}}\mathbf{f}_{\ell+1} + \mathbf{d}_\ell^{(1)}, \mu/\rho\right)$
6: $\quad \boldsymbol{\nu}_{\ell+1}^{(2)} = \text{Soft}\left(\mathbf{\Psi}^T\mathbf{f}_{\ell+1} + \mathbf{d}_\ell^{(2)}, \tau/\rho\right)$
7: $\quad \mathbf{d}_{\ell+1}^{(1)} = \mathbf{d}_\ell^{(1)} + \boldsymbol{\mathcal{L}}\mathbf{f}_{\ell+1} - \boldsymbol{\nu}_{\ell+1}^{(1)}$
8: $\quad \mathbf{d}_{\ell+1}^{(2)} = \mathbf{d}_\ell^{(2)} + \mathbf{\Phi}\mathbf{f}_{\ell+1} - \boldsymbol{\nu}_{\ell+1}^{(2)}$
9: **until** some stopping criterion is satisfied
10: **return** $\mathbf{f}_{\ell+1}$

4. SIMULATION RESULTS

Two CASSI systems were considered to generate the low spatial/high spectral and high spatial/low spectral resolution measurements $\mathbf{y}_H$ and $\mathbf{y}_M$. Both systems used the same high-resolution image, which was compressed by two ways, using spatial and spectral degradations, respectively. The matrix $\mathbf{\Phi}$ was designed using the method described in Section 2.2. The reference image considered in this paper is the classical ROSIS image acquired over Pavia, northern Italy [15] reduced to 256×256 pixels and 92 bands. The HS data cube was obtained by applying a 5×5 Gaussian lowpass filter in each band and by using a 4:1 decimation ratio ($p = 2$). Similarly, the MS datacube was generated by using a 4:1 decimation ratio ($q = 4$). Algorithm 1 was then used to estimate the image $\mathbf{f}$. The value of τ was selected by cross-validation and we found that the interval [1e-2,1e-3] provides good and similar results

for the estimated image. The parameters μ and ρ were selected as suggested in [16], and the dictionary $\mathbf{\Psi}$ was selected as a Wavelet basis. Fig. 3 (Left) shows the reconstruction results in terms of PSNR for the proposed fusion approach and the expensive high spatio-spectral resolution CASSI as a function of the compression ratio $(KM(N+L-1)/NML)$. These results were obtained using random patterned masks (denoted as "Random") and masks chosen using the procedure detailed in Section 2.2 (denoted as "Uniform"). We can observe that the PSNR increases as the compression ratio increases, as expected. The results obtained with uniform sampling are better than those obtained with random sampling. Fig. 3 (right) compares the performance of both approaches in the presence of noise for a compression ratio of 36%, as a function of the signal to noise ratio (SNR) defined as SNR $= 10\log_{10}(\mu_y/\sigma_{\text{noise}})$, where μ_y is the mean value of the measurement vector $\boldsymbol{y}$ and σ_{noise} is the noise standard deviation. Despite the loss in reconstruction quality, the proposed fusion approach provides a PSNR close to 34dB for SNR ≥ 20 dB, which is very promising. The advantage of the proposed method is to provide image reconstructions close to the ones obtained with the high-resolution CASSI but with a smaller number of measurements

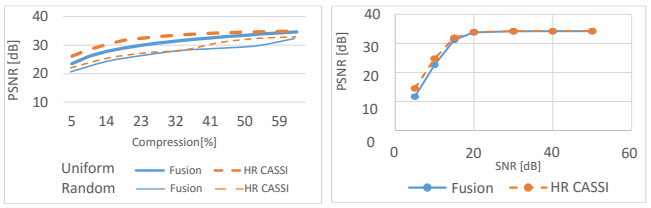

Fig. 3. (Left) PSNR [dB] comparison between a single high-resolution CASSI and the fusion of two low-resolution CASSI reconstructions. (Right) Fusion performance using CASSI in presence of noise.

The last simulation results displayed in Figs. 4 and 5 show that the proposed fusion method provides a reconstructed image close to the reference image. For instance, the spectral signatures of two particular pixels displayed in Fig. 4 are close to the references and the spatial resolution of the estimated image in Fig. 5(c) is satisfactory.

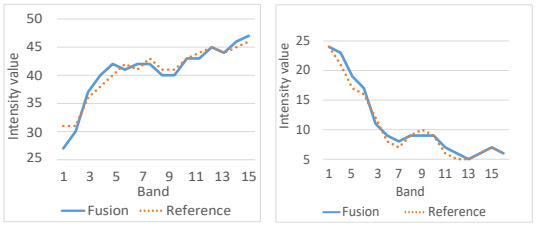

Fig. 4. Spectral fusion results. (Left) Spectral signature of pixel $\#(89, 169)$. (Right) Spectral signature of pixel $\#(124, 253)$. (Proposed in blue and reference in red).

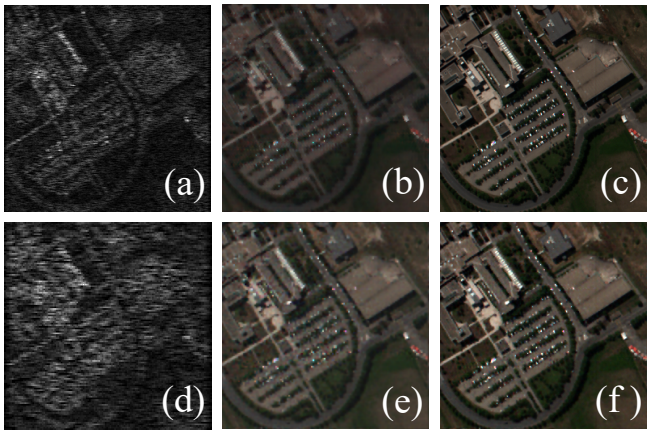

Fig. 5. Spatial fusion results. (a) Compressed HS measurements. (b) Reconstruction from HS measurements (PSRN=28 dB). (c) Proposed fusion method (PSNR=34 dB). (d) Compressed MS measurements. (e) Reconstruction from MS measurements (PSNR=29 dB). (f) Reference image.

In terms of computational complexity, the number of operations per iteration in Algorithm 1 depends on the underlying signal size and the size of the measurement vector (see [17] for more details). In particular, the algorithm in HR-CASSI performs approximately $O(K(MN)^2L)$ operations per iteration to recover an $M \times N \times L$ data cube using K sensor measurements. Similarly, the proposed fusion approach performs $O\big(K\big((\frac{MN}{p^2})^2L + (MN)^2\frac{L}{q}\big)\big)$ operations per iteration. Thus, the computational complexity is reduced depending on the values of the two decimation ratios p and q without impacting significantly the reconstruction quality.

5. CONCLUSIONS

This paper showed that compressive CASSI projections can be used to fuse high spectral/low spatial and high spatial/low spectral resolution images without the need of expensive image reconstruction. Our experiments showed that compressive sensing-based algorithms can be used to reconstruct images with high spatial and spectral resolutions using as few as 50% of data acquired by multiple sensors. In this work, the simulations obtained with the CASSI system yielded reconstructed images with PSNRs larger than 35dB, which is comparable with those obtained with high-resolution CASSI measurements, even in the presence of noise. The advantage of the proposed fusion rule is the reduced cost of the acquisition system and the reduced computational complexity of the reconstruction method. Future work includes the study of methods allowing the hyperparameters to be automatically estimated from the data, as the ones presented in [18].

6. REFERENCES

[1] J. M. Bioucas-Dias, A. Plaza, G. Camps-Valls, P. Scheunders, N. Nasrabadi, and J. Chanussot, "Hyperspectral Remote Sensing Data Analysis and Future Challenges," *IEEE Geosci. Remote Sens. Mag.*, vol. 1, no. 2, pp. 6–36, 2013.

[2] G. R. Arce, D. J. Brady, L. Carin, H. Arguello, and D. S. Kittle, "Compressive coded aperture spectral imaging: An introduction," *IEEE Signal Process. Mag.*, vol. 31, no. 1, pp. 105–115, Jan 2014.

[3] H. Arguello and G. R. Arce, "Colored coded aperture design by concentration of measure in compressive spectral imaging," *IEEE Trans. Image Process.*, vol. 23, no. 4, pp. 1896–1908, April 2014.

[4] E. J. Candes and M. B. Wakin, "An introduction to compressive sampling," *IEEE Signal Process. Mag.*, vol. 25, no. 2, pp. 21–30, March 2008.

[5] G. R. Arce, D. J. Brady, L. Carin, H. Arguello, and D. S. Kittle, "Compressive coded aperture spectral imaging: An introduction," *IEEE Signal Process. Mag.*, vol. 31, no. 1, pp. 105–115, Jan 2014.

[6] Q. Wei, J. Bioucas-Dias, N. Dobigeon, and J.-Y. Tourneret, "Hyperspectral and multispectral image fusion based on a sparse representation," *IEEE Trans. Geosci. Remote Sens.*, vol. 53, no. 7, pp. 3658–3668, July 2015.

[7] D. Needell and R. Ward, "Stable image reconstruction using total variation minimization," *SIAM Journal on Imaging Sciences*, vol. 6, no. 2, pp. 1035–1058, 2013.

[8] A. Wagadarikar, R. John, R. Willett, and D. Brady, "Single disperser design for coded aperture snapshot spectral imaging.," *Appl. Opt.*, vol. 47, no. 10, pp. B44–51, Apr. 2008.

[9] C. V. Correa, H. Arguello, and G. R. Arce, "Spatiotemporal blue noise coded aperture design for multi-shot compressive spectral imaging," *J. Opt. Soc. Am. A*, vol. 33, no. 12, pp. 2312–2322, Dec 2016.

[10] B. Li, L. Zhang, T. Kirubarajan, and S. Rajan, "Projection matrix design using prior information in compressive sensing," *Signal Processing*, vol. 135, pp. 36 – 47, 2017.

[11] H. Bai, G. Li, S. Li, Q. Li, Q. Jiang, and L. Chang, "Alternating optimization of sensing matrix and sparsifying dictionary for compressed sensing," *IEEE Transactions on Signal Processing*, vol. 63, no. 6, pp. 1581–1594, March 2015.

[12] A. P. Cuadros, C. Peitsch, H. Arguello, and G. R. Arce, "Coded aperture optimization for compressive x-ray tomosynthesis," *Opt. Express*, vol. 23, no. 25, pp. 32788–32802, Dec 2015.

[13] S. Boyd, N. Parikh, E. Chu, B. Peleato, and Jonathan Eckstein, "Distributed optimization and statistical learning via the alternating direction method of multipliers," *Found. Trends Mach. Learn.*, vol. 3, no. 1, pp. 1–122, Jan. 2011.

[14] N. B. Bras, J. Bioucas-Dias, R. C. Martins, and A. C. Serra, "An alternating direction algorithm for total variation reconstruction of distributed parameters," *IEEE Transactions on Image Processing*, vol. 21, no. 6, pp. 3004–3016, June 2012.

[15] B. Kunkel, F. Blechinger, D. Viehmann, H. Van Der Piepen, and R. Doerffer, "ROSIS imaging spectrometer and its potential for ocean parameter measurements (airborne and space-borne)," *Int. J. of Remote Sens.*, vol. 12, no. 4, pp. 753–761, 1991.

[16] M. V. Afonso, J. M. Bioucas-Dias, and M. A. T. Figueiredo, "An augmented lagrangian approach to the constrained optimization formulation of imaging inverse problems," *IEEE Trans. Image Process.*, vol. 20, no. 3, Mar. 2011.

[17] H. Arguello, C. V. Correa, and G. R. Arce, "Fast lapped block reconstructions in compressive spectral imaging," *Appl. Opt.*, vol. 52, no. 10, pp. D32–D45, Apr 2013.

[18] M. Peyrera, P. Schniter, E. Chouzenoux, J.-C. Pesquet, J.-Y. Tourneret, A. Hero, and S. McLaughlin, "Tutorial on stochastic simulation and optimization methods in signal processing," *IEEE J. Sel. Topics Signal Process.*, vol. 10, no. 2, pp. 224–241, Mar. 2016.